

# Quantum Monte Carlo study of positron lifetimes in solids

K. A. Simula, J. E. Muff, and I. Makkonen

*Department of Physics, P. O. Box 43, FI-00014 University of Helsinki, Finland*

N. D. Drummond

*Department of Physics, Lancaster University, Lancaster LA1 4YB, United Kingdom*

(Dated: March 11, 2022)

We present an analysis of positron lifetimes in solids with unprecedented depth and accuracy. Instead of approximating many-body effects as local, we study wave functions with long-range correlations included. This proves to be of crucial importance in understanding positron annihilation in metals, insulators and semiconductors. By using a new quantum Monte Carlo approach for prediction of positron lifetimes, an improved accuracy compared to previous computations is obtained for a representative set of materials when compared with experiment.

Positron annihilation is an elementary component of quantum electrodynamics [1]. Measurable annihilation parameters such as positron annihilation rate and momentum density of annihilation radiation are governed by many-body interactions between the positron and the surrounding electronic system. Theoretical predictions and experimental measurements can provide a good match for few-electron systems, for example the binding energies of positrons bound to atoms can be reproduced [2]. Theoretical studies of homogeneous electron-positron systems provide a starting point for understanding positron annihilation in more complex systems [3, 4], but real, inhomogeneous systems are nevertheless often problematic. Better description of the correlations is needed to improve theory and applicability of positron physics.

Positron annihilation spectroscopy [5] is a powerful, nondestructive method for studying systems including metals, alloys, semiconductors and insulators [6], polymers and soft matter [7, 8], and porous materials [9]. The method involves injecting positrons into a sample where they first thermalize rapidly, and then either continue diffusing as a delocalized wave or become trapped in void-like open volumes. Eventually each positron annihilates with an electron, emitting two detectable 511 keV  $\gamma$  photons. As the positrons are very sensitive to open volumes within a sample, measured lifetime components and their intensities provide information on the size and concentration of vacancies trapping the positrons [5].

Positron lifetime techniques can be combined with, for example, *in situ* irradiation [10] or optical illumination [11] to study damage production and various defect properties. Pulsed slow positron beams [12] can be used for lifetime studies of thin films or even for scanning surfaces with a micrometer-scale lateral resolution [13]. Also the study of pore size distribution in thin films is possible [9]. On the other hand, the local electronic momentum density of the annihilation site is directly connected to the Doppler broadening of the annihilation  $\gamma$  radiation, enabling the study of the chemical surroundings of lattice defects [5] or Fermi surfaces of metals [14].

Theoretical models associate measured lifetime components to microscopic traps in the material. Single-particle models, such as Hartree-Fock (HF) theory, ignore many-body correlation effects between particles. Such models predict smaller positron-electron overlaps, overestimating the positron lifetime values by nearly an order of magnitude [15]. Better description of positrons is provided by two-component density functional theory (DFT) [3], where the many-body correlation effects are included in approximate correlation functionals of the particle densities. In the local density approximation (LDA), the electron-positron correlation energies are obtained from functionals of the local densities, and the electron-positron overlap enhanced by correlations is computed with another local functional, the so-called enhancement factor. There exist also several generalized gradient approximations (GGA) [16–18] that can improve the agreement of lifetime predictions in comparison to the underlying LDA parametrizations.

Despite successes with LDA or GGA functionals, DFT is an insufficient theory for positron annihilation studies. A correlation functional may accurately predict the lifetime in some systems while failing in others. The lifetime estimates of different functionals for a given system can differ even by 30 ps (see below). Moreover, there is no *a priori* means to determine a functional best suited for a given task but experimental benchmarking is needed; and the construction of a functional can require both higher level calculations, such as quantum Monte Carlo calculations [4], and fits to experimental data [18].

For a given positron lifetime setup, the statistical accuracy that can be achieved for a defect-free sample is on the order of 1 ps. In general DFT does not reach this accuracy. Development of a practical many-body theory has been a long-standing problem in the field of positron physics and its applications. More accurate many-body theory could both improve the applicability of positron annihilation and provide new research areas. For example, the correlation functionals could be evaluated and improved using a more descriptive theory. A many-body theory also enables the study of positrons in systems

with multideterminantal nature, impossible with current methods but unavoidable with many lattice defects [19].

Importantly, the dependence of positron lifetime on lattice vibrations is an important theoretical question unaddressed to date, and should clearly be studied for complete understanding of positron annihilation in solids.

We present quantum Monte Carlo (QMC) as a new, improved method for simulations of positrons in solids. To our knowledge, this is the first QMC study of positrons in real crystals, although such studies exist for molecules [20, 21] and electron gases [4]. Calculation of positron lifetimes in the perfect bulk of materials is the first and the most critical test for benchmarking how well the electron-positron correlations in inhomogeneous solid-state systems can be described before we move on to other experimentally relevant quantities such as the momentum density of annihilating pairs. Annihilation studies in defect systems, such as vacancies, in which also the detailed ionic structure in the presence of the trapped positron plays a role, can follow after we have validated the capability of QMC to describe correlations in well-defined defect-free lattices.

We perform a detailed study of finite size effects involved and how to best describe annihilation with core electrons. Besides QMC we study vibrational effects on positron lifetime.

The studies were performed for C and Si in the diamond structure, body-centered cubic (bcc) Li, and wurtzite (wz) AlN, a set that consists of materials of past and present interest in the field of positron annihilation spectroscopy and includes insulators (C), semiconductors (AlN, Si) and metals (Li). The choice of the test set was limited by the need of experimental reference data and by the available pseudopotentials. Si and AlN have well-known experimental reference results. C is a less correlated system and expected to be easy to model with QMC. The positron lifetime in Li has been overestimated by many state-of-the-art two-component DFT correlation functionals, making the results by QMC theoretically interesting.

We use variational and diffusion Monte Carlo (VMC and DMC) methods [22, 23] as implemented in the CASINO code [24, 25]. The fermion-sign problem is treated in DMC by imposing a fixed-node approximation [26] that constrains the nodal surface of the wave function to be that of the VMC-optimized wave function.

The VMC many-body wave functions are represented as Slater-Jastrow (SJ) or Slater-Jastrow-backflow (SJB) wave functions [27, 28]. The former is a product of single-particle Slater determinants and a Jastrow factor. The determinants fix the nodal surface, and the Jastrow factor is a parametrized function describing the interparticle correlations. The SJB wave function goes beyond the single-particle SJ nodal surface by introducing parametrized shifts into the particle coordinates. Optimizing backflow parameters both increases variational

freedom in VMC and reduces the DMC fixed-node error.

The trial wave functions can be written for a system with one positron as

$$\begin{aligned}\Psi_{SJ}(\mathbf{R}) &= e^{J(\mathbf{R})} [\phi^l(\mathbf{r}_{i\uparrow})] [\phi^m(\mathbf{r}_{j\downarrow})] \phi(\mathbf{r}_+), \\ \Psi_{SJB}(\mathbf{R}) &= e^{J(\mathbf{R})} [\phi^l(\mathbf{r}_{i\uparrow} - \boldsymbol{\xi}_{i\uparrow}(\mathbf{R}))] [\phi^m(\mathbf{r}_{j\downarrow} - \boldsymbol{\xi}_{j\downarrow}(\mathbf{R}))] \\ &\quad \times \phi(\mathbf{r}_+ - \boldsymbol{\xi}_+(\mathbf{R})),\end{aligned}\quad (1)$$

where  $\mathbf{r}_\uparrow$ ,  $\mathbf{r}_\downarrow$  and  $\mathbf{r}_+$  denote the positions of up- and down-spin electrons and the positron, respectively.  $N$  is the number of particles in the system.  $\mathbf{R}$  is a  $3N$ -dimensional vector of the particle coordinates.  $J(\mathbf{R})$  and  $\boldsymbol{\xi}(\mathbf{R})$  are the Jastrow exponent and backflow displacement, respectively, parametrized with respect to different spin groupings. The  $\phi$ -functions are single-particle Kohn-Sham orbitals [29], computed with DFT using the PWSCF package of the Quantum ESPRESSO project [30] and our own positron package [31]. We assume that the delocalized positron density does not affect the average electron density and take the zero-positron-density limit of the e-p correlation energy functional [32]. The [...] signs denote Slater determinants over the orbitals. The Perdew-Burke-Ernzerhof [33] GGA and Boroninski-Nieminen [3] LDA functionals were used to solve electron and positron orbitals, respectively. The orbitals were in a localized B spline, or blip, basis [34] (see Supplemental material).

Periodic boundary conditions generalize the definition of orbitals in Eq. (1). Each orbital of band  $j$  at wave vector  $\mathbf{k}$   $\phi_{\mathbf{k}}^j(\mathbf{r})$  is of the form  $u_{\mathbf{k}}^j(\mathbf{r})e^{i\mathbf{k}\cdot\mathbf{r}}$ , i.e., a lattice periodic function  $u$  multiplied by a plane-wave exponential, according to Bloch's theorem. We use twist averaging, i.e. average results computed in grid of Bloch  $\mathbf{k}$ -vectors, but the positron orbital is always chosen from the minimum of the parabolic positron band ( $\mathbf{k} = 0$ ), as we focus on a single thermalized positron in an infinite lattice.

The Jastrow factor contains terms representing 1, 2, and 3-body correlations [35], and the backflow function contains 1 and 2-body terms. The Jastrow factor is optimized with a variance minimization method (except when core electrons are included we use energy minimization, see below) [36] and the backflow is optimized together with the Jastrow factor with an energy minimization algorithm [37].

Multiple finite-size effects bias our simulations. The long-range correlations are not described correctly by finite cell sizes, and quasirandom finite-size noise arising from the forcing of Friedel oscillations to be commensurate with the simulation cell is difficult to remove from the calculation [25]. Momentum integrals are treated as discrete sums, increasing the kinetic energy bias [38]. Noise due to discrete momentum grid is reduced by twist averaging [39]. The relaxation energies are computed by fitting computed energies to the twist vectors [25] (see Supplemental material). Finite-size effects due to long-range interactions can be reduced by increasing the

simulation cell size. Coulombic interactions are treated as Ewald sums, with a constant negative background charge to compensate the positive total charge due to the positron.

There are also systematic finite-size errors in energy arising from the positron interacting with its periodic images. In metallic systems these errors should be small when the simulation cell is large compared to the Thomas-Fermi screening length. In semiconductors the error decreases with increasing simulation cell size as  $v_M/2\epsilon$ , where  $v_M$  is the Madelung constant of the simulation cell that falls off with increasing number of atoms as  $1/N^{1/3}$  for a given cell shape, and  $\epsilon$  is the dielectric constant [25].

Norm-conserving, nonlocal Dirac-Fock average relativistic effective pseudopotentials (AREP)[40, 41] are mainly used to approximate the ion cores. The positron-nucleus interactions are calculated with inverted electron pseudopotentials. We also computed lifetimes in Si with SJ wavefunctions using effective core potential (ECP) [42] pseudopotentials with 2 electrons within the frozen core, and performed an all-electron SJ calculation for Li, enforcing cusp conditions on the electron and positron orbitals by adding short-ranged functions [43].

The electron-positron annihilation results from the overlap of electrons and the positron in the many-body wave function [44]. The annihilation rate for  $2\gamma$  annihilation is (second form given in units of  $\text{ns}^{-1}$ )

$$\Gamma = \pi r_0^2 c \sum_{i=1}^{N_e} \frac{\langle \Psi | \hat{O}_i^s \delta(\mathbf{r}_i - \mathbf{r}_+) | \Psi \rangle}{\langle \Psi | \Psi \rangle} = 100.9 g(0) \frac{N_e^\uparrow}{V}, \quad (2)$$

where  $r_0$  is the classical electron radius,  $c$  is the speed of light *in vacuo*,  $N_e$  ( $N_e^\uparrow$ ) is the number of individual (spin-up) electrons,  $V$  is the volume of the simulation cell and  $\hat{O}_i^s$  is the spin-projection operator to the singlet state of the positron-electron pair.  $g(0)$  is rotationally and translationally averaged contact pair correlation function (PCF). In the case of metals (here Li), we make an asymptotic correction [45] and multiply the PCF with  $N_e/(N_e - 1)$  to ensure that the effective electronic density is unchanged far from the positron in the simulation cell.

The system-averaged PCF  $g(|\mathbf{r}_e - \mathbf{r}_p|)$  is sampled with QMC by binning electron-positron distances. The leading-order errors in  $\Psi_{\text{VMC}}$  are removed by extrapolating the final result as  $g(r) = 2g_{\text{DMC}}(r) - g_{\text{VMC}}(r)$  [46]. The estimate of  $g(|\mathbf{r}_e - \mathbf{r}_p|)$  has poor statistics near the contact region  $|\mathbf{r}_e - \mathbf{r}_p| \approx 0$ . We estimate the  $g(0)$  by fitting a  $N$ th-order polynomial  $p(r) = a_0 - r + a_2 r^2 + \dots + a_N r^N$  to  $\log(g(r))$  in the range  $0 < r < r_{\text{cut}}$ , so that  $g(0) = \exp(a_0)$ . By setting  $a_1 = -1$  in the polynomial we assure that the fitted  $\exp(p(r))$  satisfies the Kimball cusp conditions [47]. Supplemental Material describes the details of the fitting procedure.

With pseudopotentials, the annihilation and screening interactions due to core electrons are not considered. We calculate reference DFT results and estimate the annihilation rate  $\Gamma_c$  due to core electrons using a number of enhancement functionals: Drummond *et al.* LDA (D-LDA)[4], Boroński-Nieminen LDA (BN-LDA)[3], Kuriplach-GGA (KUR-GGA)[17], and GGAs by Barbiellini *et al.* from Ref. [16] (B95-GGA) and [18] (B15-GGA). Hence the total annihilation rate is  $\Gamma = \Gamma_{\text{QMC}} + \Gamma_c$ .

For C and Si, we used 1,  $2 \times 2 \times 2$ , and  $3 \times 3 \times 3$  face-centered cubic (fcc) simulation cells, including 2, 16, and 54 atoms (8, 64, and 216 electrons with AREP pseudopotentials). For Si, also a  $4 \times 4 \times 4$  fcc cell with 128 atoms (512 electrons) was investigated. Cubic Li  $3 \times 3 \times 3$  or  $5 \times 5 \times 5$  cells had 54 or 125 atoms, with one valence electron per atom. AlN was modeled with 1,  $2 \times 2 \times 1$ , and  $3 \times 3 \times 2$  hexagonal primitive cells, resulting in 4-, 16-, and 72-atom (16-, 64-, and 288-electron) supercells. ECP pseudopotential and all-electron calculations had 3 times more electrons per atom than in AREP simulations.

We have also studied the convergence of the positron relaxation energy, defined as the energy difference between a system with and without the positron,  $E_r = E_+ - E_-$ .

The vibrational effects were studied with DFT. We calculated the dynamical matrix and diagonalized it in order to obtain the eigenfrequencies and modes of the atomic vibrations in a simulation cell. At temperature  $T$ , we sampled a set of occupied states out of the Boltzmann distribution. Displacements were sampled with the Neumann algorithm based on the occupied states. By repeatedly occupying vibrational states and sampling atomic displacements we produced a set of atomic configurations distributed according to the occupied phonon modes in the material. The lifetimes affected by vibrations were then obtained as the average lifetimes of the sampled configurations.

Figure 1 shows the QMC results of relaxation energies,  $g(0)$  and lifetimes as a function of electron number. The Monte Carlo errors are shown in the errorbars. Lifetimes of DFT predictions and from experiment are also included. Twist averaging was done in a  $\Gamma$ -centered  $4 \times 4 \times 4$  grid in the irreducible wedge of the Brillouin zone of the supercells. The backflow function was optimized separately for each twist, but with SJ wave functions the Jastrow factor optimized in the  $\Gamma$ -point was used for all of the twists. B15-GGA was used to approximate  $\Gamma_c$ . Other functionals gave mainly similar results (see Supplemental Material). ECP pseudopotential and all-electron results are shown against AREP results with the same number of atoms.

In AlN, Si and Li the backflow decreases the relaxation energy by 100–200 meV, and increases it by 200 meV in C. The larger cell size increases the relaxation energy by approximately 600 (C), 400 (AlN), 25 (Si) and 150 (Li)

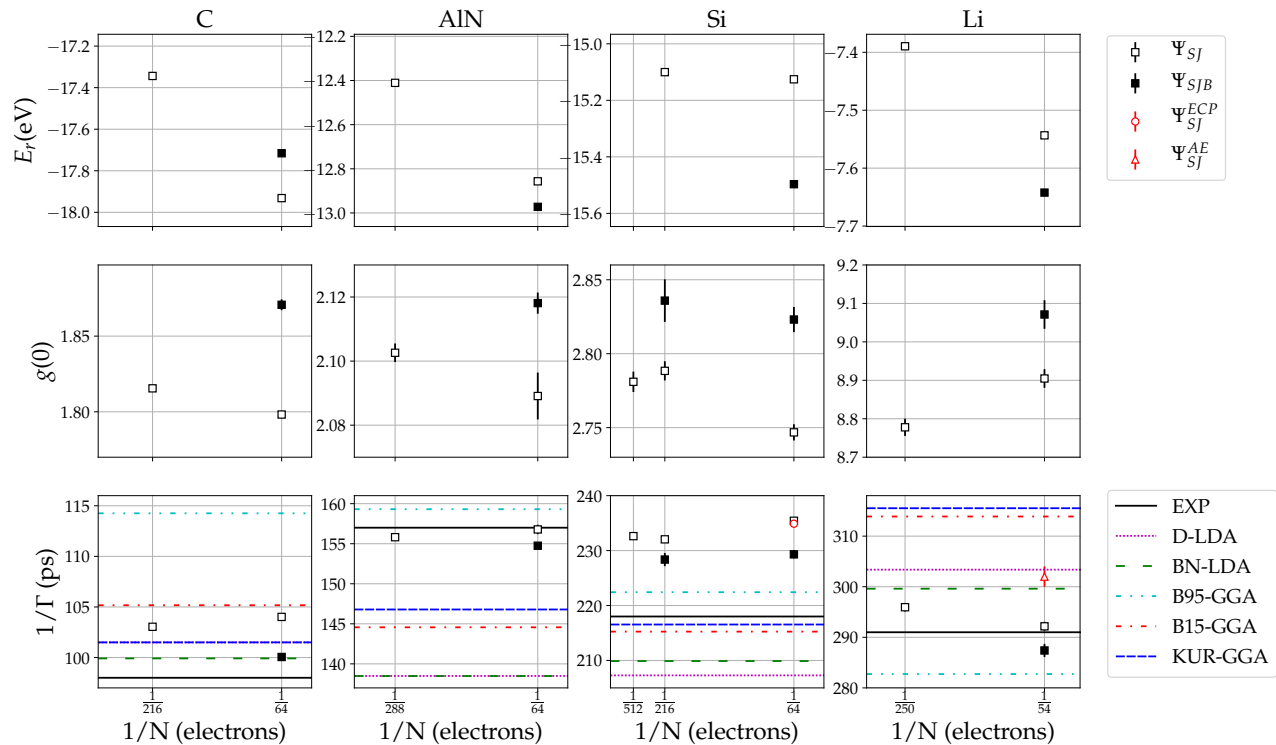


FIG. 1. Positron relaxation energies (top row), contact pair correlation functions (center row), and lifetimes (bottom row) for C, AlN, Si, and Li. The figure shows twisted SJ (empty square) and SJB (full square) wave function results with AREP pseudopotentials as well as the ECP pseudopotential (red circle) and all-electron SJ results (red triangle) as a function of the inverse of the number of electrons in the simulation. The ECP-pseudopotential and all-electron results are compared against AREP results with the same cell sizes. Monte Carlo errorbars are shown for each result. We present the lifetime estimates against experiment (black solid line) for C [48], AlN [49], Si [50], and Li [51]. We also computed DFT lifetime estimates with different positron correlation functionals (dash-dotted lines): D-LDA (violet), BN-LDA (green), B95-GGA (cyan), B15-GGA (red), and KUR-GGA (blue).

meV. The backflow increases the  $g(0)$  values. Only in Si we see convergence in PCF with respect to cell size, but changes in  $g(0)$  and lifetimes between different cell sizes of the same material are small.

In the largest cells with SJB wave functions, QMC with AREP pseudopotentials overestimates the experimental lifetimes by 2 and 10 ps in C and Si and underestimates them by 2 and 4 ps in AlN and Li. The larger cells with SJ wave functions decreased the lifetimes in C, AlN and Si by 1 ps and increased by 4 ps in Li. In Si, SJ ECP and core-corrected AREP pseudopotential results agree within errorbars. The all-electron lifetime of Li provides a 10 ps increase to the core-corrected AREP result.

The core-corrected SJB results with AREP pseudopotentials and the reference experimental values are gathered in Table I. See Supplemental Material for QMC results without core corrections and the corrections by different DFT functionals.

The SJB lifetime predictions in C and AlN match al-

TABLE I. The largest-cell SJB lifetime results obtained with AREP pseudopotentials and core corrections against experimental lifetimes.

	Lifetime (ps)	Exp. reference (ps)
C	100.1(2)	98 [48]
AlN	154.8(3)	157 [49]
Si	228(1)	218 [50]
Li	287(1)	291 [51]

most perfectly with experimental values. Li matches also very well, but the all-electron SJB result could be overestimating the experimental value by 7–10 ps, based on the SJ results, although it has to be noted that measurements on Li in the literature are scarce and old. The overestimation in Si (and Li) might result from the omission of relativistic and bound-state effects in Eq. (2) (both beyond the scope of the present Letter), finite size effects, fixed node errors, core electron approximations or

vibrational effects. Finite-size effects have been studied above. Because the backflow decreases the lifetime estimate, the QMC results are not converged with respect to the variational freedom in the wave function, and further improvements might be obtained by e.g. multideterminant wave functions. The ECP and all-electron calculations with SJB wave functions cannot be computed with current computing resources. To study vibrations, we sampled 100 atomic configurations according to the occupied phonon modes in 0 and 300 K in cubic 64-atom Si simulation cell. In both temperatures increase of lifetime due to lattice vibrations was almost negligible, 2(1) ps (see Supplement).

There is no DFT functional capable of reaching an accuracy for this set of test materials comparable with QMC. The QMC method is parameter free whereas all of the GGA functionals apart from B15-GGA involve one semiempiric parameter that has been determined by fitting to experimental lifetime data [16, 17]. The LDA construction is unique and parameter-free but the LDA simply does not work for the positron lifetime.

In conclusion, we have successfully simulated electron-positron wave functions and predicted the positron lifetimes in crystalline C, Si, Li, and AlN with QMC, with an analysis of the finite size effects. We studied different pseudopotentials and included an all-electron calculation. Also the possibility of vibrational effects greatly effecting positron lifetimes was ruled out. The results presented together with lifetimes computed by a number of DFT functionals show a systematic improvement of QMC compared to all previous methods.

The results suggest that positron lifetime spectroscopy should always use many-body calculations such as QMC to back the experimental studies. The largest simulation cells in this study are applicable to vacancy calculations, and thus the presented method can be applied effectively to support all fields of modern positron annihilation spectroscopy.

We acknowledge the generous computational resources provided by CSC (Finnish IT Centre for Science) and the use of DECI resource Archer based in Edinburgh, UK, with support from the PRACE aisbl. This work was partially supported by the Academy of Finland grants No. 285809, 293932, 319178, 334706, and 334707.

---

[1] R. A. Ferrell, Theory of positron annihilation in solids, *Rev. Mod. Phys.* **28**, 308 (1956).  
 [2] J. Mitroy, M. W. J. Bromley, and G. G. Ryzhikh, Positron and positronium binding to atoms, *J. Phys. B: At. Mol. Opt. Phys.* **35**, R81 (2002).  
 [3] E. Boroński and R. M. Nieminen, Electron-positron density-functional theory, *Phys. Rev. B* **34**, 3820 (1986).  
 [4] N. D. Drummond, P. López Ríos, R. J. Needs, and C. J. Pickard, Quantum Monte Carlo study of a positron in an

electron gas, *Phys. Rev. Lett.* **107**, 207402 (2011).  
 [5] F. Tuomisto and I. Makkonen, Defect identification in semiconductors with positron annihilation: experiment and theory, *Rev. Mod. Phys.* **85**, 1583 (2013).  
 [6] R. Krause-Rehberg and H. S. Leipner, *Positron annihilation in semiconductors: defect studies*, Vol. 127 (Springer Science & Business Media, 1999).  
 [7] R. A. Pethrick, Positron annihilation—a probe for nanoscale voids and free volume?, *Prog. Polym. Sci.* **22**, 1 (1997).  
 [8] Y. C. Jean, P. E. Mallon, and D. M. Schrader, *Principles and Applications of Positron and Positronium Chemistry* (World Scientific, 2003).  
 [9] D. Gidley, W. Frieze, T. Dull, J. Sun, A. Yee, C. Nguyen, and D. Yoon, Determination of pore-size distribution in low-dielectric thin films, *Appl. Phys. Lett.* **76**, 1282 (2000).  
 [10] N. Segercrantz, J. Slotte, F. Tuomisto, K. Mizohata, and J. Räisänen, Instability of the Sb vacancy in GaSb, *Phys. Rev. B* **95**, 184103 (2017).  
 [11] J.-M. Mäki, F. Tuomisto, A. Varpula, D. Fisher, R. U. A. Khan, and P. M. Martineau, Time dependence of charge transfer processes in diamond studied with positrons, *Phys. Rev. Lett.* **107**, 217403 (2011).  
 [12] D. Schödlbauer, G. Kögel, P. Sperr, and W. Triftshäuser, Lifetime measurements with a pulsed slow positron beam, *Phys. Status Solidi (a)* **102**, 549 (1987).  
 [13] A. David, G. Kögel, P. Sperr, and W. Triftshäuser, Lifetime measurements with a scanning positron microscope, *Phys. Rev. Lett.* **87**, 067402 (2001).  
 [14] G. Kontrym-Sznajd, Fermiology via the electron momentum distribution, *Low Temp. Phys.* **35**, 599 (2009).  
 [15] In the HF theory the particles are uncorrelated and the contact pair correlation function is  $g(0) = 1$ . However, in correlated simulations the value increases as demonstrated in Fig. 1.  
 [16] B. Barbiellini, M. J. Puska, T. Torsti, and R. M. Nieminen, Gradient correction for positron states in solids, *Phys. Rev. B* **51**, 7341 (1995).  
 [17] J. Kuriplach and B. Barbiellini, Improved generalized gradient approximation for positron states in solids, *Phys. Rev. B* **89**, 155111 (2014).  
 [18] B. Barbiellini and J. Kuriplach, Proposed parameter-free model for interpreting the measured positron annihilation spectra of materials using a generalized gradient approximation, *Phys. Rev. Lett.* **114**, 147401 (2015).  
 [19] R. Q. Hood, P. Kent, R. Needs, and P. Briddon, Quantum monte carlo study of the optical and diffusive properties of the vacancy defect in diamond, *Phys. Rev. Lett.* **91**, 076403 (2003).  
 [20] Y. Kita, R. Maezono, M. Tachikawa, M. Towler, and R. J. Needs, Ab initio quantum Monte Carlo study of the positronic hydrogen cyanide molecule, *J. Chem. Phys.* **131**, 134310 (2009).  
 [21] Y. Kita, M. Tachikawa, N. D. Drummond, and R. J. Needs, A variational Monte Carlo study of positronic compounds using inhomogeneous backflow transformations, *Chem. Lett.* **39**, 1136 (2010).  
 [22] D. M. Ceperley and B. J. Alder, Ground state of the electron gas by a stochastic method, *Phys. Rev. Lett.* **45**, 566 (1980).  
 [23] W. M. C. Foulkes, L. Mitas, R. J. Needs, and G. Rajagopal, Quantum Monte Carlo simulations of solids, *Rev. Mod. Phys.* **73**, 33 (2001).

- [24] R. J. Needs, M. D. Towler, N. D. Drummond, and P. López Ríos, Continuum variational and diffusion quantum Monte Carlo calculations, *J. Phys.: Condens. Matter* **22**, 023201 (2009).
- [25] R. J. Needs, M. D. Towler, N. D. Drummond, P. López Ríos, and J. R. Trail, Variational and diffusion quantum Monte Carlo calculations with the CASINO code, *J. Chem. Phys.* **152**, 154106 (2020).
- [26] J. B. Anderson, A random-walk simulation of the Schrödinger equation:  $H_3^+$ , *J. Chem. Phys.* **63**, 1499 (1975).
- [27] R. Jastrow, Many-body problem with strong forces, *Phys. Rev.* **98**, 1479 (1955).
- [28] P. López Ríos, A. Ma, N. D. Drummond, M. D. Towler, and R. J. Needs, Inhomogeneous backflow transformations in quantum Monte Carlo calculations, *Phys. Rev. E* **74**, 066701 (2006).
- [29] W. Kohn and L. J. Sham, Self-consistent equations including exchange and correlation effects, *Phys. Rev.* **140**, A1133 (1965).
- [30] P. Giannozzi, S. Baroni, N. Bonini, M. Calandra, R. Car, C. Cavazzoni, D. Ceresoli, G. L. Chiarotti, M. Cococcioni, I. Dabo, *et al.*, Quantum ESPRESSO: a modular and open-source software project for quantum simulations of materials, *J. Phys.: Condens. Matter* **21**, 395502 (2009).
- [31] T. Torsti, T. Eirola, J. Enkovaara, T. Hakala, P. Havu, V. Havu, T. Höynälänmaa, J. Ignatius, M. Lyly, I. Makkonen, *et al.*, Three real-space discretization techniques in electronic structure calculations, *Phys. Status Solidi (b)* **243**, 1016 (2006).
- [32] I. Makkonen, M. Hakala, and M. J. Puska, Modeling the momentum distributions of annihilating electron-positron pairs in solids, *Phys. Rev. B* **73**, 035103 (2006).
- [33] J. P. Perdew, K. Burke, and M. Ernzerhof, Generalized gradient approximation made simple, *Phys. Rev. Lett.* **77**, 3865 (1996).
- [34] D. Alfè and M. J. Gillan, Efficient localized basis set for quantum Monte Carlo calculations on condensed matter, *Phys. Rev. B* **70**, 161101 (2004).
- [35] N. D. Drummond, M. D. Towler, and R. J. Needs, Jastrow correlation factor for atoms, molecules, and solids, *Phys. Rev. B* **70**, 235119 (2004).
- [36] N. D. Drummond and R. J. Needs, Variance-minimization scheme for optimizing Jastrow factors, *Phys. Rev. B* **72**, 085124 (2005).
- [37] C. Umrigar, J. Toulouse, C. Filippi, S. Sorella, and R. G. Hennig, Alleviation of the fermion-sign problem by optimization of many-body wave functions, *Phys. Rev. Lett.* **98**, 110201 (2007).
- [38] M. Holzmann, R. C. Clay III, M. A. Morales, N. M. Tubman, D. M. Ceperley, and C. Pierleoni, Theory of finite size effects for electronic quantum Monte Carlo calculations of liquids and solids, *Phys. Rev. B* **94**, 035126 (2016).
- [39] C. Lin, F. H. Zong, and D. M. Ceperley, Twist-averaged boundary conditions in continuum quantum Monte Carlo algorithms, *Phys. Rev. E* **64**, 016702 (2001).
- [40] J. R. Trail and R. J. Needs, Smooth relativistic Hartree-Fock pseudopotentials for H to Ba and Lu to Hg, *J. Chem. Phys.* **122**, 174109 (2005).
- [41] J. R. Trail and R. J. Needs, Norm-conserving Hartree-Fock pseudopotentials and their asymptotic behavior, *J. Chem. Phys.* **122**, 014112 (2005).
- [42] M. C. Bennett, G. Wang, A. Annaberdiyev, C. A. Melton, L. Shulenburg, and L. Mitas, A new generation of effective core potentials from correlated calculations: 2nd row elements, *J. Chem. Phys.* **149**, 104108 (2018).
- [43] A. Ma, M. D. Towler, N. D. Drummond, and R. J. Needs, Scheme for adding electron-nucleus cusps to gaussian orbitals, *J. Chem. Phys.* **122**, 224322 (2005).
- [44] G. F. Gribakin, J. A. Young, and C. M. Surko, Positron-molecule interactions: Resonant attachment, annihilation, and bound states, *Rev. Mod. Phys.* **82**, 2557 (2010).
- [45] N. D. Drummond, P. López Ríos, C. J. Pickard, and R. J. Needs, First-principles method for impurities in quantum fluids: Positron in an electron gas, *Phys. Rev. B* **82**, 035107 (2010).
- [46] D. M. Ceperley and M. H. Kalos, *Monte Carlo methods in Statistical Physics* (Springer, Berlin, 1979).
- [47] J. C. Kimball, Short-range correlations and electron-gas response functions, *Phys. Rev. A* **7**, 1648 (1973).
- [48] A. Pu, T. Bretagnon, D. Kerr, and S. Dannefaer, Positron annihilation investigation of vacancies in as-grown and electron-irradiated diamonds, *Diam. Relat. Mater.* **9**, 1450 (2000).
- [49] F. Tuomisto, J.-M. Mäki, T. Y. Chemekova, Y. N. Makarov, O. V. Avdeev, E. N. Mokhov, A. S. Segal, M. G. Ramm, S. Davis, G. Huminic, *et al.*, Characterization of bulk AlN crystals with positron annihilation spectroscopy, *J. Cryst. Growth* **310**, 3998 (2008).
- [50] J. Mäkinen, P. Hautojärvi, and C. Corbel, Positron annihilation and the charge states of the phosphorus-vacancy pair in silicon, *J. Phys.: Condens. Matter* **4**, 5137 (1992).
- [51] H. Weisberg and S. Berko, Positron lifetimes in metals, *Phys. Rev.* **154**, 249 (1967).

# Supplemental Material: Quantum Monte Carlo Study of Positron Lifetimes in Solids

K. A. Simula, J. E. Muff, and I. Makkonen

*Department of Physics, P. O. Box 43, FI-00014 University of Helsinki, Finland*

N. D. Drummond

*Department of Physics, Lancaster University, Lancaster LA1 4YB, United Kingdom*

(Dated: March 11, 2022)

## Preparation of trial wave functions

We used the PWSCF package of Quantum ESPRESSO [1] to solve the single-electron orbitals to be used in constructing the Slater determinants for the QMC wave functions. For each system, we studied the sufficient plane-wave cutoff with 1 meV/atom convergence criterion. With this criterion, the all-electron simulation for Li required unpractically large plane-wave cutoffs. We then studied the convergence of the DMC energy, with cusps imposed on the orbitals by adding short-ranged functions [2], for the Li cell as a function of the DFT plane-wave cutoff and chose the plane-wave cutoff to be used in further calculation based on the 1 meV/atom convergence criterion. The chosen cutoff energies are reported in Table I.

TABLE I. The used plane-wave cutoffs in the PWSCF calculations.

System	C AREP	AlN AREP	Si AREP	Si ECP	Li AREP	Li all-electron
Cutoff (eV)	2900	5400	1400	12000	820	19000

For C and Si we used a 2-atom face-centered cubic, for AlN a 4-atom hexagonal and for Li a 2-atom cubic unit cell. To prepare trial wave functions for  $n \times m \times l$  simulation cell, the orbitals were solved by applying a  $n \times m \times l$   $\mathbf{k}$  vector grid in the unit cell simulation. The cubic simulation cell with 8 Si atoms and AREP pseudopotentials had the same convergent cutoff as the fcc cell.

After we had solved the one-electron orbitals with PWSCF, we solved the positron orbital within the potential of the obtained electron density by using our two-component DFT positron simulation package, and added it to the QMC trial wave function. The trial wave function given by PWSCF and atsup was represented as Slater determinant of the electron and positron orbitals, which were in turn represented by plane-wave sums before the blip conversion.

## Wave function optimizations

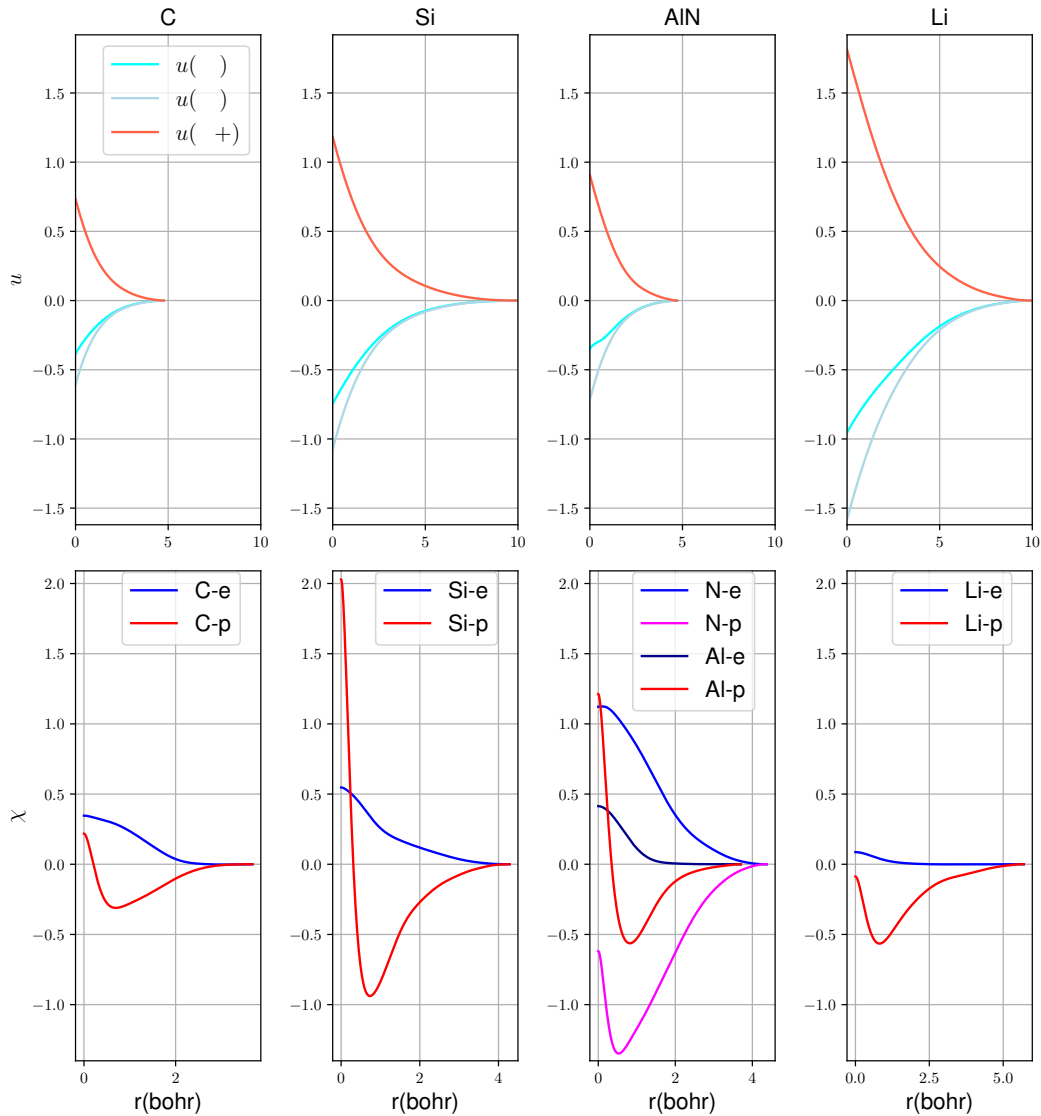
We used Jastrow exponent,  $J$ , containing polynomial electron-electron and electron-positron terms  $u$ , electron-nucleus and positron-nucleus terms  $\chi$ , and electron-electron-nucleus or electron-positron-nucleus terms  $f$ . We also used backflow functions with corresponding polynomial particle-particle and particle-nucleus terms. Table II shows the number of parameters optimized for the Jastrow factor and the backflow function with different materials. The numbers in the table are the total number of parameters in the Jastrow factor, so that the parameters in different particle groupings are summed together. Optimizations with higher number of parameters were not found to decrease the system energy.

The optimizations of the Jastrow factors were performed with variance minimization, and the backflow was optimized with energy minimization. With ECP pseudopotentials and in all-electron simulations the variance minimization led to acceptance rates of  $\approx 57\%$  for the positron in the VMC simulations. The use of energy minimization fixed the acceptance rate to 50% and lowered the obtained energy and errorbars, and was hence chosen for the computations with ECP pseudopotentials or all-electron simulations.

Figure 1 shows the  $u$ - and  $\chi$ -terms for optimized SJB systems of different materials. The Jastrow factors are taken from 16-atom C, 54-atom Si, 16-atom AlN, and 54-atom Li systems, as these systems were found to give convergent positron relaxation energies. In all of the cases we have approximately  $u_{\uparrow\downarrow} = -u_{\uparrow+}$ . We can see that the strength of the correlation effects captured by the  $u$ -term increases as C-AlN-Si-Li.  $\chi$ -term shows that the electron-nucleus correlations are always described by a monotonically decreasing function of the particle-nucleus distance. The

TABLE II. The number of parameters in the Jastrow factor and backflow function.

Jastrow	$u$	$\chi$	$f$
C	48	24	78
Si	60	24	78
AlN	36	24	78
Li	24	16	24
Backflow	$\eta$	$\mu$	
C	18	12	
Si	12	8	
AlN	18	12	
Li	12	8	

FIG. 1. The forms of the  $u$ - and  $\chi$ -terms in the Jastrow factor for Si, C, AlN, and Li.

correlations between positron and the nuclei have attractive maximum values at contact in case of C, Si and Al atoms, but the N and Li atoms seems to have repulsive correlations with the positron at all distances. The correlations in the  $\chi$ -term for positron-nucleus correlation experience a minimum at distances 0.7(C), 0.73(Si), 0.8(Al), 0.5(N), and 0.81(Li) atomic units. Clearly the strongest minimum is experienced in the case of N. One should note that the particle-nucleus correlations are very small for C and Li when compared against the other atoms studied. Also the



positron-Si correlations are very large at contact: ten times the value of contact correlations between positron and C and twice the value of the contact correlation of positron and Al, even though the electron-nucleus correlations are larger for Al than Si.

### Vibrational effects on positron lifetime

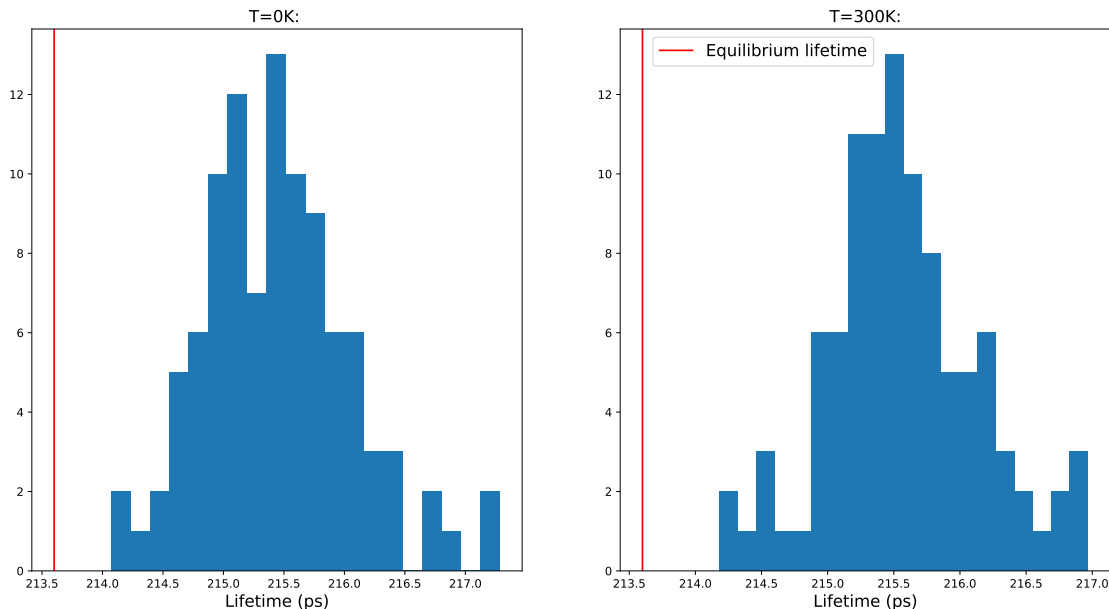


FIG. 2. Distribution of BN-LDA positron lifetimes of bulk Si in diamond structure at  $T = 0$  (left) and  $T = 300$  K (right).

In order to solve the dynamical matrix and vibrational normal modes for a 64 atom cubic Si cell we used the PWSCF package [1] with the PBE functional. First, we optimized the plane-wave cutoff within the desired accuracy, then we optimized lattice vectors to such as to give minimal energy with PBE. We used  $\mathbf{k}$  grids with  $3 \times 3 \times 3$  points.

After optimizing the numerical parameters of the density functional calculation, we made a phonon calculation. We solved the vibrational modes and frequencies with Quantum Espresso's Phonon-package [1]. Then we produced 100 PWSCF input files with different atomic displacements in 2 different temperatures, 0 and 300 K, and computed the lifetimes for all of the displacements. The BN-LDA was used to describe the electron-positron correlations.

Figure 2 shows the lifetime distributions and the mean lifetimes and respective statistical errors. As can be seen, the vibrations have the effect of increasing the lifetime by  $\sim 2$  ps: while the LDA lifetime for an equilibrium atomic configuration is 213.6 ps, the lifetimes with vibrational effects are 215.4 ps (0 K) and 215.6 ps (300 K), with standard deviations of 0.6 ps at both temperatures.

### Twist averaging of energies

The twist-averaged energies are obtained by fitting [3]

$$E_{\text{QMC}}(\mathbf{k}_s) \approx E_{\text{QMC}}(TA) + b(E_{\text{DFT}}(\mathbf{k}_s) - E_{\text{DFT}}(\text{fine})) \quad (1)$$

to the QMC energy data  $E_{\text{QMC}}(\mathbf{k}_s)$  as a function of twist  $\mathbf{k}_s$  for a given size of supercell.  $E_{\text{DFT}}(\mathbf{k}_s)$  is the DFT energy with the  $\mathbf{k}$  point grid corresponding to the QMC calculation at twist  $\mathbf{k}_s$ .  $E_{\text{DFT}}(\text{fine})$  is a DFT calculation with a fine  $\mathbf{k}$  grid. The twist-averaged energy  $E_{\text{QMC}}(TA)$  and  $b$  are fitting parameters.

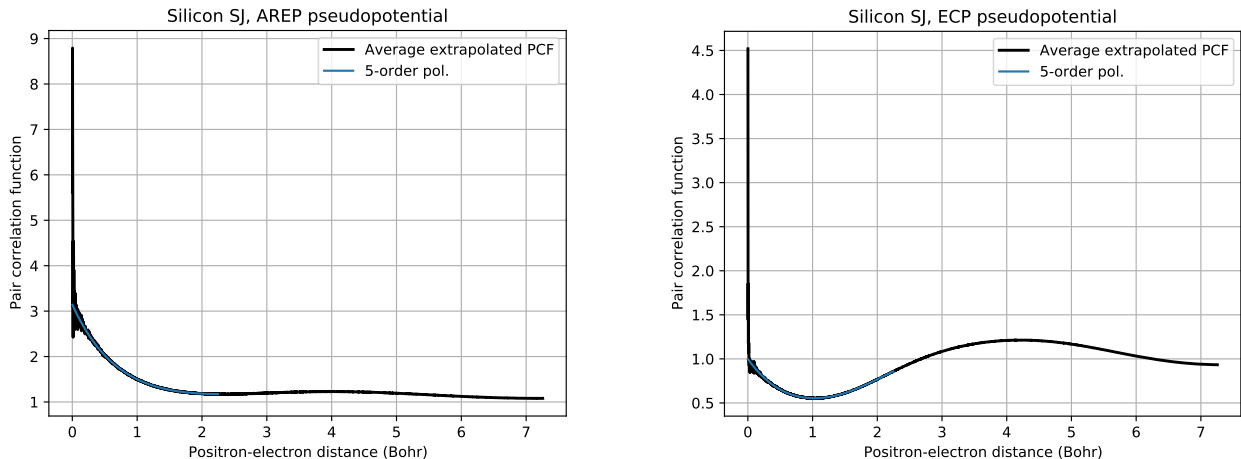


FIG. 3. Average PCF histograms, obtained by extrapolation of VMC and DMC PCF data at each twist, against the average of exponentiated fits with 5th-order polynomials. The PCF data presented here are from QMC simulations with Si SJ wavefunctions in a 16-atom fcc simulation cell, with both AREP (left) and ECP (right) pseudopotentials.

### Polynomial fits to QMC data

The PCFs were accumulated 2 times for each of the twists to get independent data. Thus for  $N_t$  twists we had  $2N_t$  independent PCF histograms  $g^i(r)$  from the VMC-DMC extrapolation. The PCF data was noisy and contained divergences close to zero positron-electron distance region, and before extrapolation we removed negative values from the extrapolated histograms. To obtain the lifetime estimates, polynomials  $p^i(r) = a_0^i + a_1^i r + \dots + a_N^i r^N$  were fitted with a chosen fitting range to each of the individual and independent  $\log(g^i(r))$  histograms by using the non-linear least-squares based Levenberg-Marquardt algorithm [4, 5]. The final estimate of the PCF at zero was taken to be the average of the exponentiated values  $\frac{1}{2N_t} \sum_{i=1}^{2N_t} \exp(a_0^i)$  at zero distance. This way we can both make the results more robust against noise near zero distances and obtain an error estimate for the contact PCFs and lifetimes. Figure 3 shows the PCF averaged over all accumulated data  $\frac{1}{2N_t} \sum_{i=1}^{2N_t} p^i(r)$  against the averaged and exponentiated fits  $\frac{1}{2N_t} \sum_{i=1}^{2N_t} \exp(p^i(r))$ , as well as the average fits with 5th-order polynomials fitted in range 0-2.25 Bohr, for the SJ Si results with AREP (left) and ECP (right) pseudopotentials.

Before fitting we had to choose the polynomial order and fitting range. For this purpose we performed a cross-validation analysis on the fitting parameters by comparing mean-squared error (MSE) estimates between individual fits against PCF data not used in the fitting. With a candidate polynomial order and fitting range, we fitted a polynomial  $p^i(r)$  to each  $2N_t$  PCF data  $g^i(r)$ . Then for each fit we computed a MSE estimate as  $E_{MSE}^i = \frac{1}{N_x} \sum_{n=1}^{N_x} [g^i(x_n) - p^i(x_n)]^2$ , where  $N_x$  is the number of columns in the PCF histograms, and  $x_n$  is the distance related to  $n$ th histogram. The index  $j$  denotes the PCF histogram corresponding to the same twist as  $g^i$ , but obtained from an independent QMC simulation. The final cross-validation MSE estimate was obtained as  $E_{MSE}^{CV} = \frac{1}{N_t} \sum_{i=1}^{N_t} E_{MSE}^i$ . We computed this estimate with varying polynomial order and fitting range for each material, cell size, pseudopotential (including the all-electron calculation), and wave function approximation. An example of our cross-validation results on silicon with SJB wave function in the 54-atom simulation cell can be seen in Fig. 4.

The lowest  $E_{MSE}^{CV}$  were obtained in C, AlN and Si with 7th-order polynomials at fitting ranges of 3.5-5 Bohr. However, with 5th-order polynomials and fitting ranges of 2 (C), 2.2 (AlN) and 2.5 (Si), the cross-validation errors were within 1% of the lowest value with 7th-order polynomial. In Li, the lowest cross-validation error values were obtained with 5th-order polynomials at all distances, with the fitting range of  $\approx 5$  Bohr giving the lowest value, with slight variation between wave function approximations, simulation cell sizes and core electron approximations. Again, the 5th-order polynomial with fitting range of 2.25 Bohr gave cross-validation errors that were within 1% of the lowest value.

We wanted to use the same method for all of our PCF data for consistency. Based on the findings listed above we chose to use 5th-order polynomial and fitting range of 2.25 Bohr, as this provided robust results with all materials, gave a cross validation error within 1% of the best value in all systems, and was a fit to relatively small distance and polynomial order hence preventing any catastrophic errors from occurring. Results obtained by fitting in each system

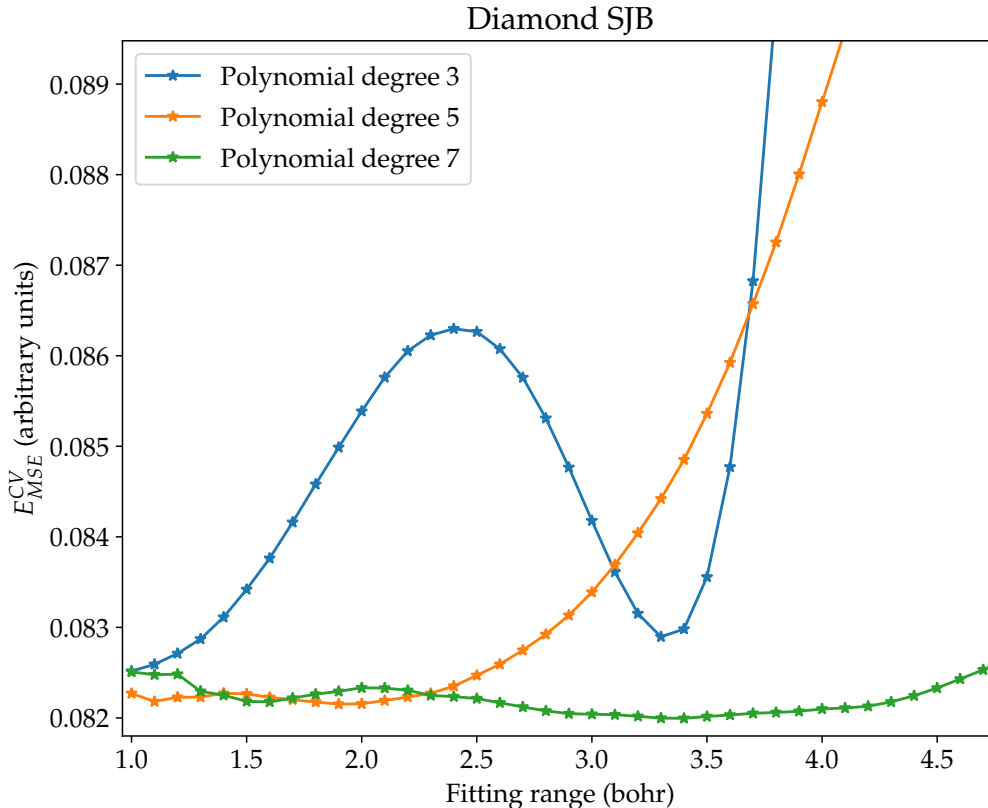


FIG. 4. Results of a cross-validation analysis on the fitting parameters with different polynomial orders and fitting ranges for a C 16-atom simulation cell and SJB wave function.

with polynomial order and fitting range giving the minimal  $E_{MSE}^{CV}$  provided to be the same with our chosen method, with respect to Monte Carlo errorbars.

### Core corrections

Table III presents lifetime estimates (valence annihilation only) of DFT and QMC calculations, as well as the core-corrected AREP QMC estimates with different density functionals. The experimental lifetimes are shown for comparison. The C and AlN estimates are taken from the 64-electron, the Si estimate from the 216-electron and the Li estimate from the 54-electron simulation cell with twisted SJB wave functions. Li is an exception, as different density functionals both under- and overestimate the QMC result. For all of the materials except Li, the core-corrected QMC lifetime estimates seem to be relatively robust against the choice of functional for the core correction, as the lifetime estimates are with different core correction functionals within the range of  $\sim 2$  ps, which is only a little larger than the statistical error on the results.

- 
- [1] P. Giannozzi, S. Baroni, N. Bonini, M. Calandra, R. Car, C. Cavazzoni, D. Ceresoli, G. L. Chiarotti, M. Cococcioni, I. Dabo, *et al.*, *J. Phys.: Condens. Matter* **21**, 395502 (2009).
- [2] A. Ma, M. D. Towler, N. D. Drummond, and R. J. Needs, *J. Chem. Phys.* **122**, 224322 (2005).
- [3] R. J. Needs, M. D. Towler, N. D. Drummond, P. López Ríos, and J. R. Trail, *J. Chem. Phys.* **152**, 154106 (2020).
- [4] D. W. Marquardt, *J. Soc. Ind. Appl. Math.* **11**, 431 (1963).
- [5] K. Levenberg, *J Numer Anal* **16**, 588 (1944).

TABLE III. Lifetimes computed with DFT and QMC with AREP pseudopotentials against experimental values. The predictions with only valence electrons are considered for different DFT functionals and QMC for C ( $\tau_{\text{valence}}^{\text{C}}$ ), AlN ( $\tau_{\text{valence}}^{\text{AlN}}$ ), Si ( $\tau_{\text{valence}}^{\text{Si}}$ ) and Li ( $\tau_{\text{valence}}^{\text{Li}}$ ). Below the lines with valence-only lifetime estimates for each material the core-corrected lifetime predictions are presented, computed as  $\tau_{\text{full}} = (\Gamma_c + \Gamma_v)^{-1}$ , where the core annihilation rate is estimated with the DFT functional of the corresponding column, and the valence rate is from the QMC simulation.

	D-LDA	BN-LDA	B95-GGA	B15-GGA	KUR-GGA	QMC	Experiment
$\tau_{\text{valence}}^{\text{C}}$ (ps)	103.3	101.8	115.9	107.0	103.3	101.7(2)	
$\tau_{\text{full}}^{\text{C}}$ (ps)	100.0(2)	99.8(2)	100.4(2)	100.1(2)	100.0(2)		98[6]
$\tau_{\text{valence}}^{\text{AlN}}$ (ps)	147.7	148.1	166.9	153.6	155.5	165.1(3)	
$\tau_{\text{full}}^{\text{AlN}}$ (ps)	153.7(3)	153.3(3)	157.7(3)	154.8(3)	155.4(3)		157[7]
$\tau_{\text{valence}}^{\text{Si}}$ (ps)	214.5	217.5	228.1	223.7	223.4	237(1)	
$\tau_{\text{full}}^{\text{Si}}$ (ps)	228(1)	228(1)	231(1)	228(1)	229(1)		218[8]
$\tau_{\text{valence}}^{\text{Li}}$ (ps)	351	347	301	353	353	320(1)	
$\tau_{\text{full}}^{\text{Li}}$ (ps)	280(1)	279(1)	299(1)	287(1)	289(1)		291[9]

- [6] A. Pu, T. Bretagnon, D. Kerr, and S. Dannefaer, *Diam. Relat. Mater.* **9**, 1450 (2000).  
[7] F. Tuomisto, J.-M. Mäki, T. Y. Chemekova, Y. N. Makarov, O. V. Avdeev, E. N. Mokhov, A. S. Segal, M. G. Ramm, S. Davis, G. Humnic, *et al.*, *J. Cryst. Growth* **310**, 3998 (2008).  
[8] J. Mäkinen, P. Hautojärvi, and C. Corbel, *J. Phys.: Condens. Matter* **4**, 5137 (1992).  
[9] H. Weisberg and S. Berko, *Phys. Rev.* **154**, 249 (1967).